ULTRASONIC IMAGING **33,** 251- 263 (2011)

# Ultrasound Attenuation Measurements Using a Reference Phantom with Sound Speed Mismatch

KIBO NAM, IVAN M. ROSADO-MENDEZ, NICHOLAS C. RUBERT, ERNEST L. MADSEN, JAMES A. ZAGZEBSKI AND TIMOTHY J. HALL

*Department of Medical Physics*
*University of Wisconsin-Madison*
*1111 Highland Avenue*
*Madison, WI 53705*
*tjhall@wisc.edu*

Ultrasonic attenuation may be measured accurately with clinical systems and array transducers by using reference phantom methods (RPM) to account for diffraction and other system dependencies on echo signals. Assumptions with the RPM are that the speeds of sound in the sample ($c_{sam}$) and in the reference medium ($c_{ref}$) are the same and that they match the speed assumed in the system beamformer ($c_{bf}$). This work assesses the accuracy of attenuation measurements by the RPM when these assumptions are not met. Attenuation was measured for two homogeneous phantoms, one with a speed of sound of 1500 m/s and the other with a sound speed of 1580 m/s. Both have an attenuation coefficient approximately equal to that of the reference, in which the speed of sound is 1540 m/s. Echo signals from the samples and the reference were acquired from a Siemens S2000 scanner with a 9L4 linear array transducer. Separate acquisitions were obtained with $c_{bf}$ at its default value of 1540 m/s and when it was set at values matching the speeds of sound of the phantoms. Simulations were also performed using conditions matching those of the experiment. RPM-measured attenuation coefficients exhibited spatially-dependent biases when $c_{sam}$ differed from $c_{bf}$ and $c_{ref}$. Mean errors of 19% were seen for simulated data, with the maximum errors in attenuation measurements occurring for regions of interest near the transmit focus. Biases were minimized (mean error with simulated data was 5.6%) using $c_{bf}$ that matched $c_{sam}$ and assuring that power spectra used for attenuation computations in the sample are from precisely the same depth as those from the reference. Setting the transmit focus well beyond the depth range used to compute attenuation values minimized the bias.

Key Words: Attenuation; backscatter; beamformer; quantitative ultrasound; reference phantom method; speed of sound.

## I. INTRODUCTION

Ultrasound is widely recognized as a convenient and efficient diagnostic tool. B-mode ultrasound imaging primarily displays tissue characteristics by intensity modulating the display according to the amplitudes of echo signals. However, brightness contrast on B-mode images also depends on system settings and operator controls. Thus, tissue characteristics presented in conventional ultrasound B-mode images are interpreted relatively and subjectively.

Quantitative ultrasound has been introduced to supplement these qualitative evaluations by providing absolute and objective measurements of tissue characteristics. For example, attenuation levels of tissues are judged qualitatively on B-mode images by their degree of shadowing or on the basis of penetration depth. When measured quantitatively, attenuation has shown potential to characterize the degree of diffuse disease and remove some of the subjectivity when describing focal lesions. Measurements of ultrasound attenuation have been used to differentiate fatty liver from normal liver[1-3] and benign tumors from malignant ones[4] in the liver. Other researchers have suggested that ultrasound attenuation has diagnos-



0161-7346/11/12 $18.00

tic value in bone disease,[5,6] in predicting the condition of the cervix during pregnancy,[7] and in differential diagnosis of breast masses.[8,9] Attenuation values have also been utilized to detect and characterize thermal lesions in ablation therapy.[10]

Attenuation can be estimated from echo data derived from clinical ultrasound systems that provide unprocessed, radiofrequency (rf) echo signals.[11,12] To do so, however, system-dependent factors affecting the echo signal, such as frequency-dependent sensitivity of the transducer-pulser-receiver system and beam-focusing patterns must be accounted for. Use of a reference phantom is a straightforward way to eliminate these system-dependent factors. With the reference-phantom method[13] (RPM), one computes the ratio of echo signal power spectra from the tissue to power spectra derived at the same depth from a well-characterized reference medium. The slope of the power spectra ratio as a function of depth yields the attenuation coefficient of the tissue. The RPM provides accurate attenuation values over homogeneous tissue regions,[14] and it has been utilized successfully to measure attenuation in human liver with fatty infiltration or with cirrhosis[15,n16] and to monitor changes in canine livers resulting from glucocorticoid administration.[16]

Accounting for diffraction effects on the echo signal with the RPM requires that the speed of sound in the reference media ($c_{ref}$) must be approximately the same as that of the sample ($c_{sam}$).[13] Exact guidelines for how close the sound speeds need to be were not presented by Yao.[13] However, Tu[17] reported that a difference in speeds of sound of 2.1% resulted in substantial artifacts on attenuation-coefficient images computed using the RPM with an array transducer. Chen[18] studied degradation of resolution in phantoms whose sound speeds differed from that used in the beamformer ($c_{bf}$) of an array system. Although Chen directed his work towards spatial resolution considerations, his simulations point to mismatches in focal patterns when transmitting into media having different sound speeds and the mismatches could lead to artifacts when applying the RPM for determining attenuation. Omari et al[19] report that a hybrid technique for estimating attenuation, normalizing the echo signal power spectra from a region of interest (ROI) to the power spectrum from a reference phantom and then evaluating changes in the center frequency with depth, may be less prone to errors than the RPM when there are sound speed differences between the tissue and reference media. Omari et al[19] did not study depth dependencies of attenuation estimates, one of the problems vividly brought out by Tu's[17] work.

The goal of this paper is to investigate effects of sound-speed mismatches on attenuation estimates done using the RPM. Emphasis is given to results at different distances from the transducer as well as with different transmit focal depths. The work is applied to array transducers with electronic beamforming. We evaluate results for tissue-mimicking phantoms in which the sound speed is lower or higher than that of the reference phantom. Possible improvements in estimation accuracy are considered for cases in which the sound speed used in the system beamformer matches that of the media scanned and where steps are taken to precisely match depths in the reference and sample from which power spectra are computed and compared. Both experimental and simulation results are presented.

## II. METHODS

### Reference phantom method

For the convenience of the reader, a brief review of the RPM for estimating attenuation and backscatter levels is provided. Assuming the Born approximation, Yao et al[13] have shown that for uniform samples, the ratio of the echo signal power spectra from a sample to that from a reference medium can be described as:

$$\frac{S_{sam}(f,z)}{S_{ref}(f,z)} = \frac{G_{sam}(f,z)D_{sam}(f,z)}{G_{ref}(f,z)D_{ref}(f,z)} \frac{BSC_{sam}(f)\exp(-4\alpha_{sam}(f)z)}{BSC_{ref}(f)\exp(-4\alpha_{ref}(f)z)} \quad (1)$$

where $f$ denotes frequency and $z$ represents the depth of the ROI. $S(f,z)$ is the power spectrum of the backscattered echo signal. The subscripts *sam* and *ref* denote the sample and reference medium, respectively. $G(f,z)$ represents the signal transduction and processing in the system. $D(f,z)$ accounts for diffraction effects. $BSC(f)$ represents the backscatter coefficient in the medium, $exp(-4\alpha(f)z)$ represents the total attenuation between the transducer surface and the depth of interest and $\alpha(f)$ is the attenuation coefficient in the medium. Power spectra typically are computed by averaging periodograms within windowed regions whose axial extent might be, e.g., 4 mm. It is assumed that any differences in attenuation between the sample and reference phantom over these short signal segments do not affect computations of acoustic properties.

There are three depth-dependent parameters in Eq. (1): $G(f,z)$, $D(f,z)$, and $exp(-4\alpha(f)z)$. The RPM makes two additional assumptions related to these parameters: (a) the sound speed within the reference medium is approximately the same as that of the sample; and (b) for array systems, the sound speed used in the system's beamformer is the same as that of the sample and reference medium. With these two assumptions, Eq. (1) can be simplified to:

$$\frac{S_{sam}(f,z)}{S_{ref}(f,z)} = \frac{BSC_{sam}(f)}{BSC_{ref}(f)}\exp(-4(\alpha_{sam}(f)-\alpha_{ref}(f))z) \quad (2)$$

For an ROI with constant backscatter properties, the RPM estimates the attenuation of the sample using:

$$\alpha_{sam}(f) = -\frac{\ln\left(\frac{S_{sam}(f,z)}{S_{ref}(f,z)}\right)\Big|_{z2} - \ln\left(\frac{S_{sam}(f,z)}{S_{ref}(f,z)}\right)\Big|_{z1}}{4(z_2 - z_1)} + \alpha_{ref}(f) \quad (3)$$

where $z_2$ and $z_1$ are depths in the ROI and $z_2 > z_1$.

**Experimental phantoms**

Three tissue-mimicking homogeneous phantoms with different sound speeds were utilized. The phantoms consist of 15 cm x 5 cm x 15 cm water-based agarose gel media housed in rectangular 9 mm thick acrylic boxes. One 5 cm x 15 cm surface on each phantom is bounded with a 25 μm thick Saran-Wrap® (Dow Chemical, Midland MI, USA) scanning window. The phantoms were made with 5-43 μm diameter glass bead scatterers randomly spatially distributed in the gel, at a concentration of about 400 beads/mm$^3$. In constructing the phantoms, molten agar was prepared by mixing dry agarose powder into an n-propanol water mixture, where the n-propanol concentration was chosen to provide sound speed values of approximately 1500 m/s, 1540 m/s and 1580 m/s in the different phantoms. Graphite powder (32 g/l of molten gel) was added to provide approximately 0.5 dB/cm-MHz ultrasound attenuation in each phantom. Phantoms were rotated at 1rpm during congealing to prevent gravitational settling of particles.

**Table 1.** Sound speed and attenuation measurements of three phantoms.

| | 1500 m/s phantom | 1540 m/s phantom | 1580 m/s phantom |
|---|---|---|---|
| **Sound speed** | 1499 m/s | 1539 m/s | 1581 m/s |
| $\alpha_0$ | 0.433 dB/cm | 0.491 dB/cm | 0.524 dB/cm |
| ***n*** | 1.179 | 1.114 | 1.085 |
| **Slope of attenuation coefficient vs. frequency at 5 MHz** | 0.559 dB/cm-MHz | 0.573 dB/cm-MHz | 0.591 dB/cm-MHz |

The acoustic properties of the phantoms were measured using 2.5 cm thick, 7.6 cm diameter test samples produced at the time of construction of each phantom. Four pairs of unfocused single element transducers were used to span the 2.5-10 MHz frequency range, and a narrowband substitution method[20] was applied for both attenuation and sound speed measurements. Sound speed values were determined only at 2.5 MHz since dispersion (over the analysis frequency range) is negligible in these materials. Attenuation coefficients were fit to a power law of the form $\alpha(f) = \alpha_o f^n$ where $\alpha_o$ and $n$ are constants; resulting values for $\alpha_o$ and $n$ are shown in table 1. Measured speeds of sound also are presented in table 1. The slopes of attenuation coefficient vs. frequency are shown at 5 MHz, the approximate center frequency of echo signal power spectra obtained over the ROIs in the samples and reference phantom.

## Clinical scanner data collection

Rf echo data were collected using a Siemens Acuson S2000 system (Siemens Medical Solutions USA, Inc., Malvern, PA) with a 9L4, 192 element linear array transducer driven at a center frequency of 6 MHz. The Axius Direct ultrasound research interface on the system was used to acquire frames of rf echo data at a 40 MHz sampling frequency.[12] Each frame consisted of signals from 456 acoustic beam lines. Ten frames were acquired from each phantom, each representing data from an 8.5 cm (axial) x 3.8 cm (lateral) field of view, with an elevational translation or a rotation of the transducer between each frame to obtain statistically independent echo data. However the scan window of the phantoms was quite narrow (5 cm) so the ten frames of rf data recorded during each experiment may have been partially correlated. The same control settings, including time-gain compensation, overall gain and transmit focal distance, were used for each phantom. Separate experiments were done with transmit focal distances of 2 cm, 3 cm, 4 cm, 5 cm and 7 cm, in each experiment recording both sample and reference phantom data using the same control settings. The research interface allowed the sound speed assumed in the beamformer to be varied from the default value of 1540 m/s. Data from the 1500 m/s and 1580 m/s phantoms were recorded setting the beamformer sound speed either at 1540 m/s or equal to the sound speed of the scanned phantom.

For comparison, the experimental conditions were simulated using a frequency-domain B-mode imaging model developed in our laboratory.[21] The computational model assumes a spatially random distribution of scatterers within a medium of specified attenuation coefficient and sound speed. The program incorporates transmit focusing and dynamic receive beamforming with any desired sound speed.[18] Three homogeneous numerical phantoms with attenuation coefficients and sound speeds matching those of the physical phantoms were simulated. Each numerical phantom contained scatterers at a concentration of 10 scat-

**Table 2.** Four data acquisition and analysis cases by the variations of the beamformer sound speed, $c_{bf}$, and the depth calculation sound speed $c_z$.

| Case | Beamformer sound speed, $c_{bf}$ | Depth calculation sound speed, $c_z$ |
|---|---|---|
| **I** | 1540 m/s | 1540 m/s |
| **II** | 1540 m/s | Uses each phantom's sound speed |
| **III** | Match to each phantom's sound speed | 1540 m/s |
| **IV** | Match to each phantom's sound speed | Uses each phantom's sound speed |

terers/mm$^3$ and each of these simulated phantoms had a backscatter coefficient equal to $2x10^{-6}f^3$ cm-$^1$sr$^{-1}$, where $f$ is the frequency in MHz. The numerical phantoms were 8 cm (axial) x 4 cm (lateral) by 1cm (elevational). Sound speeds of the numerical phantoms were set to 1500 m/s, 1540 m/s, and 1580 m/s, which were within one standard deviation of measured values of sound speeds of the physical phantoms.

To enable close comparison between simulation and experiment, the measured attenuation values at 5 MHz shown in table 1 were applied to the simulated phantoms. The simulated transducer mimicked a Siemens 9L4 linear array transducer. This probe has 192 elements whose sizes are 0.18 mm (lateral) x 10 mm (elevational) with a center-to-center element spacing of 0.2 mm. Using the simulated phantoms, a single frame of rf echo data for 200 closely-spaced acoustic beam lines was generated over the 8 cm x 4 cm region that was simulated. The aperture of the transducer was adjusted to keep a constant F-number of 2 during dynamic-receive focusing. Although the clinical array transducer in the experiment has a mechanical lens providing a fixed elevational focus, the simulated transducer did not use elevational focusing. A Gaussian-shaped pulse with a center frequency of 6 MHz and a 70% bandwidth was assumed in the model.

## Four data acquisition and analysis cases

Experimentally, the 1500 m/s and the 1580 m/s phantoms were used as 'samples' while the 1540 m/s phantom served as the reference. RPM attenuation estimations were studied for four conditions, or cases, as described in table 2.

## Attenuation estimation

A ROI extending from 1-6 cm axially and 1-3 cm in width was selected from the simulated data. The near-field data from the experiment suffered from ring-down and other artifacts associated with the transducer-to-phantom surface, so the ROI in the experimental data was restricted to 1.5-6 cm (0.5 cm shorter than the ROI used in simulations). Except for this minor adjustment, the simulated data closely mimicked the experiment.

Power spectra in the sample and reference were calculated using Welch's method.[22] In this method, a segment of data spanning a depth of several millimeters axially and several A-lines laterally are processed by first applying a Hann gating window axially to the rf data, computing the Chirp Z transform[23] and then averaging laterally to produce the echo signal power spectrum over the specific 'analysis window.' This process is repeated on multiple, overlapping data segments over the entire ROI. The size of the power spectrum analysis windows used was 4 mm (axially, 5.19 μs duration using 1540 m/s) x 4 mm (laterally, 48 acoustic scan lines for experimental data and 40 scan lines for simulated data). Analysis windows were allowed to overlap by 75% both axially and laterally. The ratios of the power spectra

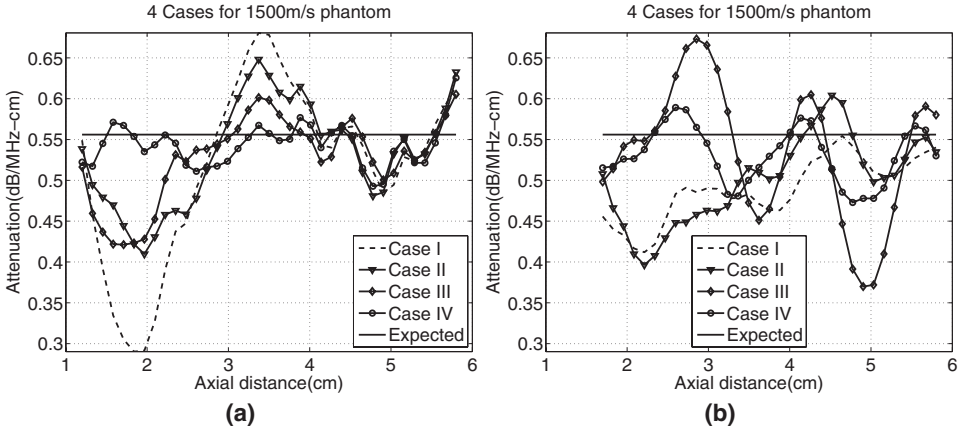


**FIG. 1** Slopes of attenuation coefficient vs. frequency over the ROI with a 2 cm transmit focal distance, for all four experimental cases (Cases I, II, III, IV) shown on each graph. Subplot (a) is from simulated data while subplot (b) shows results from experiments. The sound speed in the sample is 1500 m/s and that in the reference phantom is 1540 m/s. The model attenuation coefficients in the sample and reference phantom are 0.559 dB/cm-MHz and 0.573 dB/cm-MHz respectively (horizontal line).

from the sample to those of the reference phantom at the same depth were grouped in 8 mm segments in the axial direction and the logarithm of the ratios were fit to a straight line using a least-squares fitting routine. The slope of this line was used to estimate the attenuation coefficient (neper/cm), as shown in Eq. (3). This was done over the frequency range of 5-6 MHz and 4-8 MHz for experimental data and simulations, respectively. The frequency range used for the experimental data was limited to the 5-6 MHz bandwidth to minimize any errors that would be caused by the slightly nonlinear frequency-dependent attenuation in the phantoms, noted in table 1. However, the range used for the simulated data, where attenuation was modeled as being proportional to frequency, was 4-8 MHz to enable a greater number of independent estimates of the slope of attenuation coefficient vs. frequency. The slopes of attenuation coefficient vs. frequency were obtained by converting to dB/cm and then dividing by the frequency in MHz. The slopes of attenuation coefficient vs. frequency were obtained over the entire depth from which data were acquired.

Attenuation values were obtained with the transmit focus at 2 cm, 3 cm, 4 cm, 5 cm and 7 cm for both sample phantoms. Attenuation estimates from the same depth were averaged laterally over the ROI.

Biases of RPM results with respect to the laboratory measurements were quantified using an absolute percent error, defined as:

$$Absolute\ percent\ error(z) = \frac{\left|\alpha_{estimated}(z) - \alpha_{known}(z)\right|}{\alpha_{known}(z)} \times 100 \tag{4}$$

where $\alpha_{estimated}(z)$ and $\alpha_{known}(z)$ are the estimated attenuation coefficients using the RPM and the laboratory measurements, respectively.

## III. RESULTS

Attenuation coefficient slopes vs. depth obtained from simulated and experimental data with the transmit focus at 2 cm are presented in figure 1 for the 1500 m/s phantom and in fig-

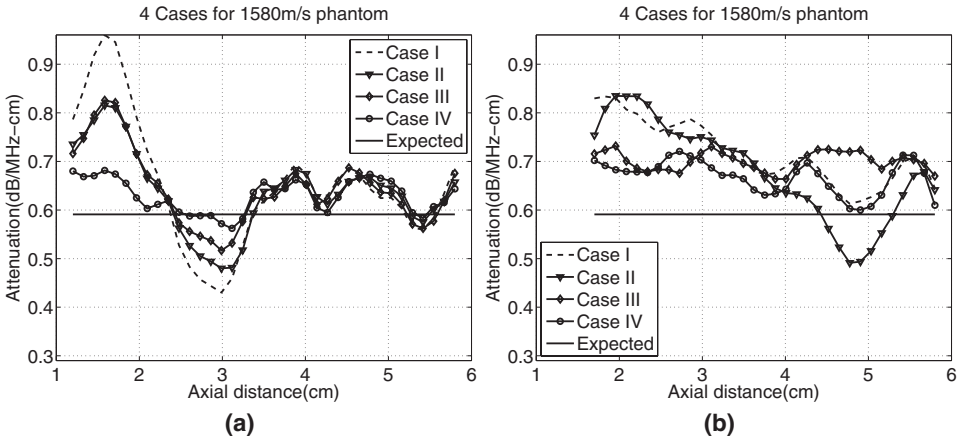


**FIG. 2** Slopes of attenuation coefficient vs. frequency over the ROI with a 2 cm transmit focal distance, for all four experimental cases (Cases I, II, III, IV) shown on each graph. Subplot (a) is from simulated data while subplot (b) shows results from experiments. The sound speed in the sample is 1580 m/s and that in the reference phantom is 1540 m/s. The model attenuation coefficients in the sample and reference phantom are 0.591 dB/cm-MHz and 0.573 dB/cm-MHz respectively (horizontal line).

ure 2 for the 1580 m/s phantom. The horizontal line in each plot indicates the expected slope of attenuation coefficient vs. frequency at 5 MHz based on through-transmission measurements made on test samples. As can be seen in figure 1, without accounting for differences in speeds of sound in the sample, beamformer and reference (Case I), significant deviations from the expected attenuation values are found, particularly near the 2 cm transmit focus simulation data. This bias is reduced somewhat with partial corrections, either by precisely matching the depths from which echo signal power spectra for the sample and reference are computed (Case II) or by applying a beamformer sound speed that accurately matched the sound speed of the sample or the reference media when data were acquired (Case III). The smallest deviations from expected values occurred for results from simulated echo data in Case IV, where both corrections schemes are applied.

Similar trends in the results from the 1580 m/s sample phantom are observed in figure 2 for the different Cases. Notice in this example, the large bias in results at the 2 cm transmit focal depth are in the opposite direction as that for the 1500 m/s case due to the opposite sound speed difference between the sample and reference. The significant improvements observed for Case IV again are observed.

The absolute percent errors for the different data acquisition and analysis cases are summarized in table 2 and presented in figure 3 for the 1500 m/s phantom and in figure 4 for the 1580 m/s phantom. In each figure, the top row of plots presents results from simulations and the bottom row shows experimental results. Each sub plot includes five curves to display results for each of the five different transmit focus locations.

As can be seen in all Case I results from simulations (upper rows in figures 3 and 4), a significant bias in the estimated attenuation results occurs near the transmit focus. The bias is larger at deeper transmit focus settings, except for the 7 cm focus setting. Experimental data from the two sample phantoms are presented in the lower rows in figures 3 and 4. The general trend in the experimental data follows that seen with simulations (the bias is the greatest near the transmit focal depth and it is reduced by applying the corrections outlined in table 2). Results from both simulation and experiment where the sound speed used in the beamformer and the sound speed assumed in the depth calibration matched the sound speed of the sample (Case IV) exhibits the smallest fluctuation in attenuation estimates over the ROI for all focal depth settings. The experimental results exhibited less variation among the four Cases than

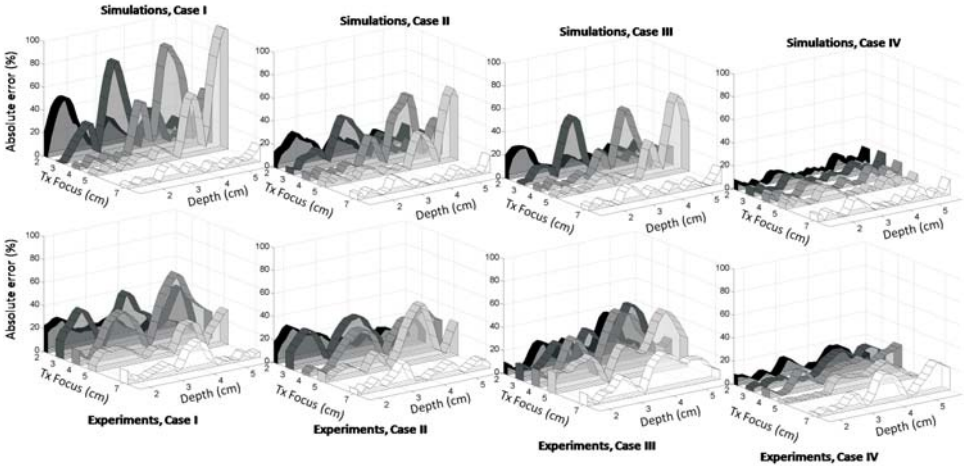


**FIG. 3** Absolute percent error of slopes of attenuation coefficient vs. frequency from Cases I, II, III, and IV (from left to right) derived from simulation (top row) and experimental (bottom row) data, where $c_{sam} = 1500$ m/s and $c_{ref} = 1540$ m/s: Case I, where no corrections are applied, i.e., $c_{bf} = 1540$ m/s for both sample and reference and $z_{sam} \neq z_{ref}$; Case II, where $c_{bf} = 1540$ m/s for both sample and reference but $z_{sam} = z_{ref}$; Case III, where $c_{bf}$ matches each *of* $c_{sam}$ and $c_{ref}$ but no depth correction is applied, $z_{sam} \neq z_{ref}$; Case IV, where $c_{bf}$ matches each *of* $c_{sam}$ and $c_{ref}$ AND sound speed corrections are used to match distances, $z_{sam} = z_{ref}$. The transmit focus settings were 2 cm, 3 cm, 4 cm, 5 cm and 7 cm. The model attenuation coefficients in the sample and reference phantom are 0.559 dB/cm-MHz and 0.573 dB/cm-MHz, respectively.

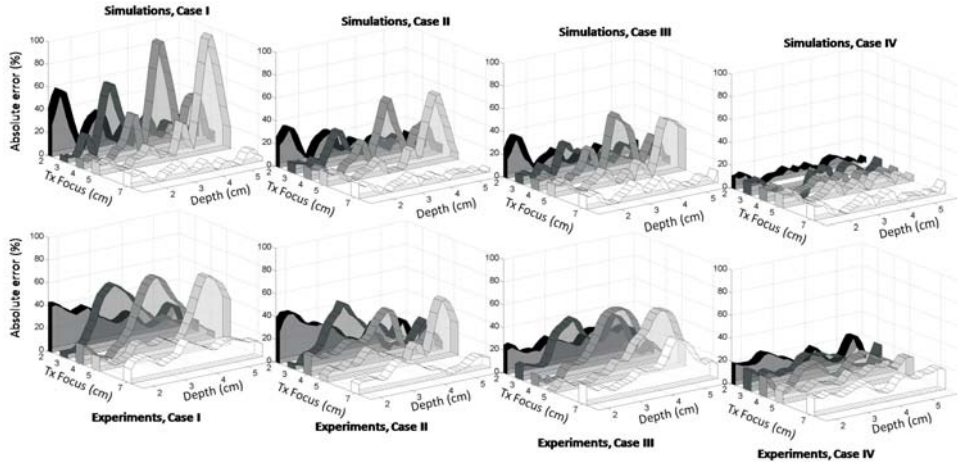


**FIG. 4** Absolute percent error of slopes of attenuation coefficient vs. frequency from Cases I, II, III, and IV (from left to right) derived from simulation (top row) and experimental (bottom row) data, where $c_{sam} = 1580$ m/s and $c_{ref} = 1540$ m/s: the Case conditions are outlined in the caption of figure 3 . The transmit focus settings were 2 cm, 3 cm, 4 cm, 5 cm and 7cm. The model attenuation coefficients in the sample and reference phantom are 0.591 dB/cm-MHz and 0.573 dB/cm-MHz, respectively.

the simulation results, possibly because of lower statistical fluctuations in the power-spectral density estimates (multiple independent frames were used for computing the attenuation for experimental data).

The attenuation coefficient was generally underestimated for the 1500 m/s phantom and overestimated for the 1580 m/s phantom when no corrections were applied. The mean error in simulated data, obtained by averaging over depth and considering all transmit focus locations, was -4.3% for the 1500 m/s phantom and 5.0% for the 1580 m/s phantom.

Interestingly, no significant difference among the four analysis cases was observed when using the 7 cm transmit focus location. Evidently, when the transmit focal zone is significantly deeper than the transducer aperture length and its location is beyond the ROI, the errors caused by mismatched sound speeds in the reference and sample are smaller than for the shallow transmit focus conditions. Focusing effects over the ROI are much more gradual for the 7 cm depth than for the other transmit focal depths, and that apparently minimizes the attenuation estimate bias errors.

## IV. DISCUSSION

The RPM provides accurate estimates of attenuation and backscatter coefficients using clinical ultrasound equipment when the speed of sound in the reference closely matches that of the sample. The focus of this paper was on the accuracy of the method when the sound speed in the reference media, used to account for system dependencies on the data, differs from the sound speed in the sample.

Three observations are noted. First, for either a sample having a sound speed of 1500 m/s or 1580 m/s, where the reference phantom's sound speed is 1540 m/s, a bias existed in the attenuation estimates, particularly near the transmit-focus location. Secondly, this bias near the transmit focus tended to be larger (the maximum error was higher) at deeper focus settings. Finally, the polarity of the bias near the transmit focus location was in opposite directions for the 1500 m/s sample results compared to those for the 1580 m/s sample.

A possible explanation of these observations is the difference in spatial power distribution between the sample and reference phantoms caused by the difference in the location of the focus accompanying the difference in speeds of sound in the sample and reference media. To visualize these power distribution differences, another set of simulations was done. Most conditions were the same as those applied in simulations described above, with the sample having either a 1500 m/s or a 1580 m/s sound speed, the reference phantom having a sound speed of 1540 m/s and the linear array dimensions matching those of the transducer used in the experiment. However, now the sample and reference media had identical attenuation properties, 0.6 dB/cm-MHz.

Power spectra were calculated from the sample and reference echo data applying both Cases I and IV, as described in table 2. Then the log of the ratio of the power from the sample to that from the reference was obtained by integrating echo signal power spectra over the 4-8 MHz frequency range. These power ratios were computed over the whole ROI and displayed as images. Results are shown in figure 5 for Case I (left column) and Case IV (right column) and are presented for transmit focus locations of 2 cm, 4 cm, and 7 cm.

Comparing the left column (Case I) with the right column (Case IV), since the sample and reference have the same attenuation and backscatter coefficients for this simulation, the expected log ratio is 0 dB throughout the image. The log ratio in Case IV exhibited a consistent pattern throughout the depth range, closer to 0 dB than that in Case I. Figures 5(a) and (c) depict a clear bias near the transmit focus location, resulting in a banding of the imaged sample-to-reference phantom power-spectra ratios. The banding is more prominent in figure 5(c), where the transmit focal depth is deeper, than in figure 5(a). The banding disappears for Case IV, where the speed of sound assumed in the beamformer closely matches that in the reference or sample media and actual sound speeds in the sample and reference are used to assure that power spectra ratios are from precisely the same depth.

The banding near the transmit focus location is caused by the slight mismatch of the locations of the focal peak in the signals from the sample and those from the reference media. The actual focal depth in the 1500 m/s phantom is slightly deeper than that in the reference medium whose speed of sound is 1540 m/s and slightly shallower in the 1580 m/s phantom.[18]

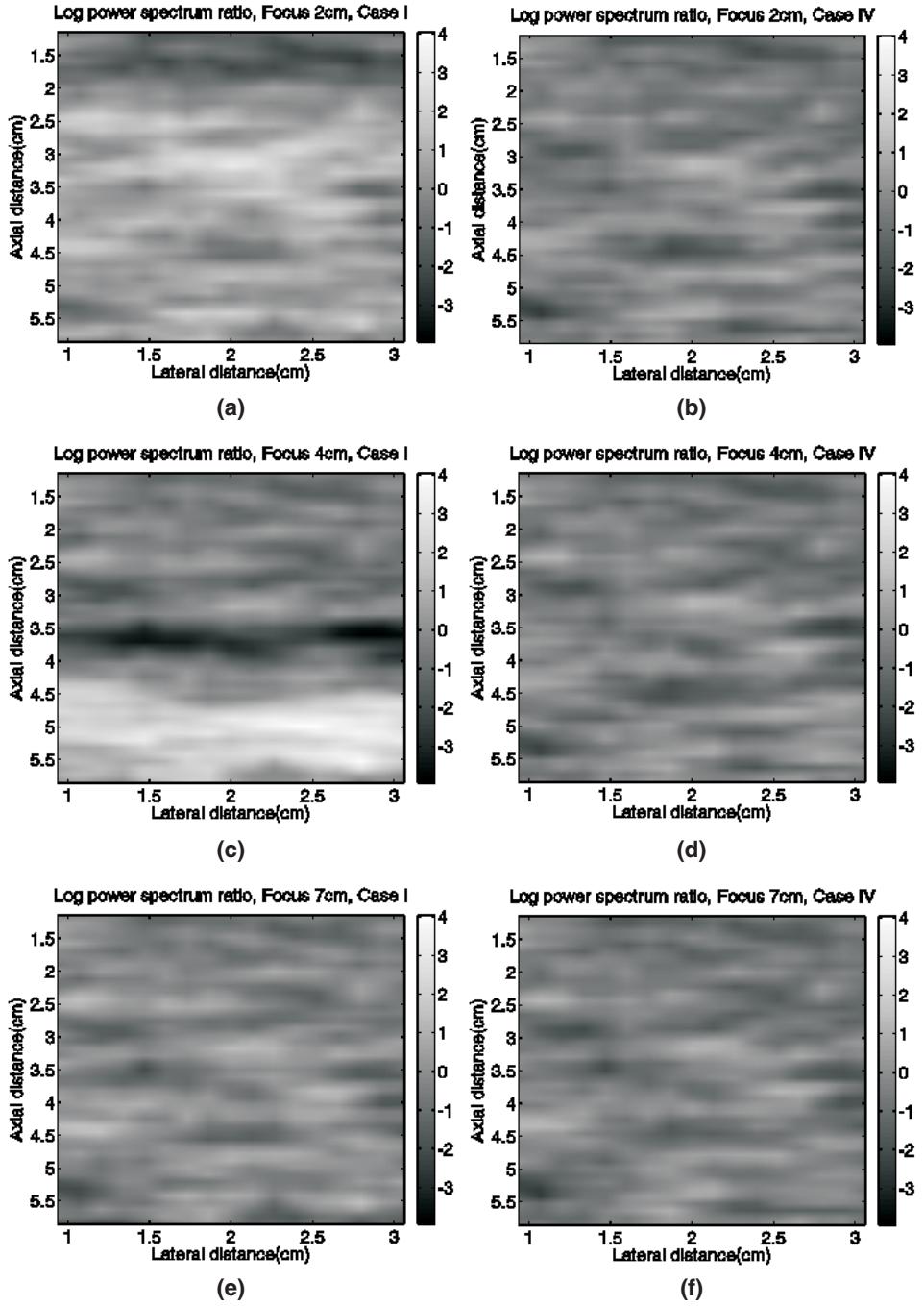


**FIG. 5** Images from simulations depicting ratios of integrated echo signal power spectra from a sample to that from corresponding locations in a reference phantom. The sample and reference phantom have identical attenuation and backscatter coefficients, but $c_{sam} = 1500$ m/s and $c_{ref} = 1540$ m/s. The ratio values are expressed in dB. (a) Case I with transmit focus at 2 cm, (b) Case IV with transmit focus at 2 cm, (c) Case I with transmit focus at 4 cm, (d) Case IV with transmit focus at 4 cm, (e) Case I with transmit focus at 7 cm and (f) Case IV with transmit focus at 7 cm.

Beyond the focus, the energy in the beam spreads gradually, further weakening the received signal. The beam energy spread occurs more rapidly with depth when the focal depth is

closer to the transducer, as in the 1580 m/s sample, than when it is deeper (1500 m/s sample). This is consistent with the observation that the average attenuation coefficients were *underestimated* by 4.3% for the 1500 m/s sample but *overestimated* by 5.0% for the 1580 m/s sample. This also explains why the bias trends near the transmit focus location in the 1500 m/s phantom and 1580 m/s phantom are in opposite directions.

The effects of a mismatch in the sound speed in the sample and reference media is not necessarily peculiar to the RPM, but likely occurs for any attenuation estimation method where power spectra ratios of sample to reference are employed to eliminate system dependent factors. Thus, methods where system calibrations are done using planar reflectors in water, for example, should be evaluated in a similar fashion.

Generally, when estimating attenuation coefficients in tissues, the sound speed in the sample will not be known exactly. Some ultrasound imaging instruments vary the beamformer sound speed depending on the tissue scanned and use of such a feature to match the beamformer sounds speed to that of the tissue may enable better estimates of parameters determined using a reference phantom. Another possibility is to use instruments that provide sound speed optimization routines, either through automated methods[24] or by allowing the operator the choice of selecting the most appropriate beamformer sound speed, when doing attenuation estimations such as these. Future studies will investigate the ability of these algorithms to supply accurate values for correcting the RPM following our Case IV approach.

Compared to examples shown in figures 5(a), 5(c) and 5(e), horizontal banding is minimized in figure 5(e) where the transmit focus is at 7 cm. This is consistent with results in figures 3 and 4, where errors caused by different sound-speed values in the sample and reference phantom appear to be lowest when the transmit focal zone is beyond the ROI for which attenuation coefficients are determined. With the transmit focus well beyond the ROI, evidently focusing differences in the sample and reference are not as significant. Alternatively, applying more weakly-focused transmissions might also minimize the focal zone bias errors. These conditions will be explored more thoroughly in future reports.

In figures 3 and 4, the experimental results exhibited higher pecent errors than simulation results for Case IV. One possible cause is the existence of electronic system noise in the rf data from the experiment. The simulated rf data did not include random noise which was present in the expemental data. Another possible cause for higher (apparent) errors in attenuation estimates from backscattered echo data is the linear dependence on frequency assumed from the narrowband substitution method. Attenuation in the simulated data had a linear frequency dependence. Finally elevational focusing in the clinical imaging system could have played a role in addition to electronic focusing in the image plane. Since this elevational focusing was done mechanically, the diffraction difference in the sample and reference caused by this focusing and sound speed mistmatch is as not accounted for in Case IV. Elevational focusing was not used in the simulations.

Finally, when comparing the attenuation estimate bias error for experimental and simulation data, the trends in the bias as a function of spatial position and sound speed difference are the same, even though there is a lack of exact agreement between these results. The differences between experiment and simulation might be caused by small differences between numerical and physical phantoms, the latter also having uncertainties associated with the values of attenuation vs. frequency. Moreover, the model did not attempt to simulate the precise frequency reponse of the system nor exact details of the transducer's elevational focusing. Its purpose was to probe whether the experimental observations were reasonable. Further, there are statistical fluctuations in the rf echo signals and corresponding power spectra that would require very large numbers of observations to obtain true expectation values (and thereby obtain 'best estimates'). Real phantoms have finite sizes, which limit the number of statistically-uncorrelated rf echo signals available. With that in mind, similar

trends in attenuation estimate bias from experimental and simulated data was all that was expected from this study. However, trends in bias error from both experiments (physical phantoms, transducers, etc.) and simulations (where few approximations are made) provided insight into the sources of these bias errors.

## V. CONCLUSIONS

Differences between the speed of sound in a sample and that assumed in the beamformer, as well as between the sound speed of a sample and that of reference medium, cause biases in RPM attenuation measurements. With array systems, the bias is greatest near the transmit focus location. Biases are reduced or eliminated by matching the sound speed assumed in the beamformer to that of the medium and taking care to match power spectra in the sample and reference from precisely the same depth. If the sound speed of the sample is unknown, setting the transmit focus location further from the ROI minimizes biases in attenuation estimates.

## ACKNOWLEDGEMENTS

This work was supported by NIH Grant R01CA111289 and the Consejo Nacional de Ciencia y Tecnologia of Mexico (Reg. 206414).

## REFERENCES

1. Fujii Y, Taniguchi N, Itoh K, et al. A new method for attenuation coefficient measurement in the liver: comparison with the spectral shift central frequency method, *J Ultrasound Med 21*, 783–788 (2002).

2. Lu ZF, Zagzebski JA, Lee FT. Ultrasound backscatter and attenuation in human liver with diffuse disease, *Ultrasound Med Biol 25*, 1047-1054 (1999).

3. Narayana PA, Ophir J. On the frequency dependence of attenuation in normal and fatty liver, *IEEE Trans Sonics Ultrason 30*, 379-383 (1983).

4. Dong BW, Wang M, Xie K, Chen MH. In vivo measurement of frequency-dependent attenuation in tumors of the liver, *J Clin Ultrasound 22*, 167-174 (1994).

5. Wear KA. Characterization of trabecular bone using the backscattered spectral centroid shift, *IEEE Trans Ultrason Ferroelectr Freq Contr 50*, 402-407 (2003).

6. Sasso M, Haćat G, Yamato Y, Naili S, Matsukawa M. Dependence of ultrasonic attenuation on bone mass and microstructure in bovine cortical bone, *J Biomech 41*, 347-355 (2008).

7. Yassin L, Bigelow TA, McFarlin BL. Estimate of the attenuation coefficient using a clinical array transducer for the detection of cervical ripening in human pregnancy, *Ultrasonics 51*, 34-39 (2011).

8. Golub RM, Parsons RE, Sigel B, et al. Differentiation of breast tumors by ultrasonic tissue characterization, *J Ultrasound Med 12*, 601-608 (1993).

9. Huang SW, Li PC. Ultrasonic computed tomography reconstruction of the attenuation coefficient using a linear array, *IEEE Trans Ultrason Ferroelectr Freq Contr 52*, 2011-2022 (2005).

10. Ribault M, Chapelon JY, Cathignol D, Gelet A. Differential attenuation imaging for the characterization of high intensity focused ultrasound lesions, *Ultrasonic Imging 20*, 160-177 (1998).

11. Wilson TA, Zagzebski JA, Varghese T, Chen Q, Rao M. The Ultrasonix 500RP: A commercial ultrasound research interface, *IEEE Trans Ultrason Ferroelectr Freq Contr 53*, 1772-1782 (2006).

12. Brunke, SS, Insana MF, Dahl JJ, et al. An ultrasound research interface for a clinical system, *IEEE Trans Ultrason Ferroelectr Freq Contr 54*, 198-210 (2007).

13. Yao LX, Zagzebski JA, Madsen EL. Backscatter coefficient measurements using a reference phantom to extract depth-dependent instrumentation factors, *Ultrasonic Imaging 12*, 58-70 (1990).

14. Bigelow BA, Labyed Y, McFarlin BL, Sen-Gupta E, O'Brien WD. Comparison of algorithms for estimating ultrasound attenuation when predicting cervical remodeling in a rat model, in *Proc IEEE Intl Symp on Biomed Imaging*, pp. 883-886 (2011).

15. Zagzebski JA, Lu ZF, Yao LX. Quantitative ultrasound imaging in vivo results in normal liver, *Ultrasonic Imaging 15*, 335-351 (1993).

16. Lu ZF, Zagzebski JA, O'Brien RT, Steinberg H. Ultrasound attenuation and backscatter in the liver during prednisone administration, *Ultrasound Med Biol 23*, 1-8 (1997).

17. Tu H. Ultrasonic attenuation imaging and analysis, in *Doctorate Dissertation* (*UW-Madison*), Chapt. 4, pp. 123-133 (2005).

18. Chen Q and Zagzebski JA. Simulation study of effects of speed of sound and attenuation on ultrasound lateral resolution, *Ultrasound Med Biol 30,* 1297-1306 (2004).

19. Omari E, Lee H, Varghese T. Theoretical and phantom based investigation of the impact of sound speed and backscatter variations on attenuation slope estimation, *Ultrasonics (*In press, 2011).

20. Madsen EL, Frank GR, Carson PL, et al. Inter-laboratory comparison of ultrasonic attenuation and speed measurementsm, *J Ultrasound Med 5*, 569-576 (1986).

21. Li Y, Zagzebski JA. A frequency domain model for generating B-mode images with array transducers, *IEEE Trans Ultrason Ferroelectr Freq Contr 46*, 690-699 (1999).

22. Welch PD. The use of fast Fourier transforms for the estimation of power spectra: A method based on time averaging over short modified periodograms, *IEEE Trans Audio Electroacoust.15*, 70-73 (1967).

23. Rabiner L, Schafer R, Rader C. The chirp z-transform algorithm, *IEEE Trans Audio Electroacoust 17*, 86-92 (1969).

24. Napolitano D, Chou CH, McLaughlin G, et al. Sound speed correction in ultrasound imaging, *Ultrasonics 44*, e43-e46 (2006).